Journal of Power Sources 202 (2012) 56–62

Contents lists available at SciVerse ScienceDirect

Journal of Power Sources

journal homepage: www.elsevier.com/locate/jpowsour

Nanostructured tungsten carbide/carbon composites synthesized by a microwave heating method as supports of platinum catalysts for methanol oxidation

Jin Lin Lu[a,b], Zi Hui Li[a,c], San Ping Jiang[b], Pei Kang Shen[c,*], Lin Li[a,**]

[a] School of Mechanical and Aerospace Engineering, Nanyang Technological University, 50 Nanyang Avenue, Singapore 639798, Singapore
[b] Fuels and Energy Technology Institute & Department of Chemical Engineering, Curtin University, Perth, WA 6102, Australia
[c] State Key Laboratory of Optoelectronic Materials and Technologies, School of Physics and Engineering, Sun Yat-Sen University, Guangzhou 510275, China

ARTICLE INFO

Article history:
Received 30 September 2011
Received in revised form 6 November 2011
Accepted 8 November 2011
Available online 17 November 2011

Keywords:
Catalyst support
Methanol oxidation reaction
Microwave heating
Tungsten carbide

ABSTRACT

In this work, a series of nanostructured tungsten carbide/carbon (WC/C_x) composites are in situ synthesized using a microwave heating method. The composites are used as platinum (Pt) catalyst supports for methanol oxidation in acid media. Their structure, composition and specific surface area are characterized by X-ray diffraction (XRD), energy dispersive spectroscopy (EDS), Raman spectroscopy, and Brunauer–Emmett–Teller (BET) measurements. Platinum catalysts supported on the WC/C_x composites are synthesized by an improved impregnation method. The electrochemical performance and stability of the catalysts are evaluated by cyclic voltammetry (CV) and chronoamperometry (CA). The $Pt/WC/C_x$ catalysts exhibit higher activity and stability than does the Pt/VC (Pt supported on carbon black Vulcan XC-72) catalyst. The results indicate that there is a synergistic effect between Pt and the WC/C_x support, which can promote the electrocatalysis of Pt for methanol oxidation reaction (MOR).

© 2011 Elsevier B.V. All rights reserved.

1. Introduction

Fuel cells have been considered as alternative clean power sources for the near future. Direct-methanol fuel cells (DMFCs) are a special type of low temperature fuel cells, and are suited for portable devices or transportation applications. In DMFCs, because methanol and water are fed directly into the cell, steam reforming is not required. Storage of methanol is much easier than hydrogen as it does not need high pressure or low temperature [1–6]. The anodic reaction in DMFCs is the oxidation of methanol to produce protons, electrons and CO_2. Currently, platinum is the most widely used catalyst for methanol electro-oxidation, but it is easily poisoned by adsorbed CO. As such, PtRu has gained a significant popularity over Pt, but the activity of PtRu for methanol oxidation still needs to be enhanced. Due to the limited supplies of both Pt and Ru, PtRu bimetallic catalysts are relatively expensive, which in turn leads to the hindrance of commercialization of DMFCs [7–10].

In order to achieve fine dispersion, high utilization and stable nanoscaled metallic particles, catalyst-supporting strategies have been explored [11]. Carbon particles are frequently used as catalyst supports because of their relative stability in both acidic and basic media, good electrical conductivity and high specific surface area. To further improve the metallic particles' catalytic activity and resistance to reactive intermediates such as CO, many efforts have been made to develop new catalyst supporting materials. For example, novel nano-structured carbon materials, such as carbon nanotubes (CNT) [2,12] and carbon nanofibers (CNF) [13] have been investigated as catalyst supports for proton exchange membrane fuel cells (PEMFCs) because of their unique structures and properties. In addition, mesoporous carbon [14], conductive diamonds [15] and conductive oxides [16] have been studied as catalyst supporting materials for PEMFCs or DMFCs.

Recently, the carbides of transition metals, especially WC, have attracted considerable attention due to their unique properties, such as stability at anodic potentials in acid solutions, exceptional resistance to poisoning, high electronic conductivity and activity toward the dissociation of methanol and water [17–20]. The activity and stability of pure WC can be further improved by formation of WC-containing composites, such as WC-silica [21] and WC-carbon [22]. Jeon et al. [23] prepared a Pt/WC/C catalyst using a high temperature reduction method. The Pt/WC/C catalyst exhibited an improved CO electrooxidation activity by giving a 42% higher specific activity for MOR as compared with the Pt/C catalyst. Wang et al. [24] synthesized a WC/graphitic carbon nanocomposite using an in situ synthetic route at 1000 °C. The Pt/WC/graphitic catalyst exhibits a mass activity of 205.6 mA mg^{-1} Pt, three times that of Pt/C. Ganesan et al. [25] investigated the platinized mesoporous

* Corresponding author.
** Corresponding author. Tel.: +65 67906285; fax: +65 67904062.
E-mail address: mlli@ntu.edu.sg (L. Li).

0378-7753/$ – see front matter © 2011 Elsevier B.V. All rights reserved.
doi:10.1016/j.jpowsour.2011.11.018

WC for MOR. The results indicated that the role of WC was not only a support for Pt, but also an active phase working together with Pt for MOR. Zhao et al. [26] prepared Pt catalysts supported on WC/multi-walled carbon nanotubes (MWCNT). The results suggested that the synergistic effect between Pt nanoparticles and WC, and the structural effect of MWCNTs gave rise to a high performance of Pt catalysts for MOR. Some differently structured WC and WC-containing materials as catalyst supports have also been investigated for hydrogen electrooxidation, ethanol electrooxidation and oxygen electroreduction [27–32]. The conventional synthetic routes using solid carbon precursors such as carbon black or carbon nanotubes often suffer from the aggregation of WC particles, leading to the damage of the original support materials and loss of activity and stability. The commonly used high temperature heating methods are time-consuming, resulting in the relatively large particle sizes and low specific surface areas.

Here, we report a novel and simple route to in situ synthesis of nanostructured WC/C_x composites using glucose as a C precursor and ammonium metatungstate as a W precursor by means of a microwave heating method, which is a versatile technique for the synthesis of nano-materials [33]. The as-prepared WC/C_x composites are used as supports of Pt catalysts. The performances of Pt/WC/C_x catalysts are investigated in detail for MOR at 25 °C in acid media.

2. Experimental

Materials used in this work include glucose (99.9% purity, $C_6H_{12}O_6$, Sigma–Aldrich), Pluronic P123 ($EO_{20}PO_{70}EO_{20}$, BASF®), ammonium metatungstate (AMT, $(NH_4)_6H_2W_{12}O_{40}{\cdot}xH_2O$, Sigma–Aldrich), hexachloroplatinic acid ($H_2PtCl_6{\cdot}xH_2O$, Sigma–Aldrich), carbon black (Vulcan XC-72, Cabot Corp.), methanol (99.99% purity, Sigma–Aldrich) and Nafion solution (5 wt.% in isopropanol and water, DuPont).

First, 5 g glucose and 0.263 g P123 (P123:glucose = 5:95 in weight) were mixed in 60 mL de-ionized water under magnetic stirring at room temperature (25 °C) for 30 min. The pH value of the above mixture was adjusted to 1 by adding 2 M HCl solution, followed by adding a certain amount of AMT. Here, the nominal molar ratios of WC:C were varied to 1:1, 1:10 and 1:20 (the final products were assigned as WC/C, WC/C_{10} and WC/C_{20}, respectively). The above mixtures were dried completely at 80 °C, followed by grinding in an agate mortar to form a fine powder. The powders were heated in a microwave oven (JJ-101) for 30 min in a nitrogen atmosphere, and then cooled to room temperature. The temperature of the reactants was monitored by an infrared temperature detector in the microwave oven. The heating temperature was set at 1000 °C, which could be achieved in 30 s. The obtained products were washed in a 2 M NaOH solution for 2 h and finally filtered with distilled water.

The catalysts were prepared using the improved impregnation method [34,35]. First, the quantitative WC/C_x composite supports were dispersed into a H_2PtCl_6 aqueous solution and the Pt loading was controlled at 20 wt.% to the supports. After ultrasonic mixing for 30 min, the suspension was stirred at 400 rpm to form a thick slurry at 25 °C, followed by drying the slurry in an oven at 60 °C. After that, the agglomerates were ground in an agate mortar. The obtained powders were heated in a tube furnace at 300 °C under a 5 vol.% H_2 balanced with Ar atmosphere for 2 h, followed by cooling to room temperature (25 °C) in nitrogen atmosphere. The Pt/VC catalyst with a Pt loading of 20 wt.% was also prepared for comparison according to the same preparation procedure.

The XRD patterns of the catalysts were obtained on an XRD-6000 diffractometer employing Cu K_α radiation (λ = 0.15418 nm) at a scan rate of 5° min^{-1} and the scan range from 20° to 80°. The composition and structure of the WC/C_x composite materials were examined by Raman spectroscopy (Renishaw® RM1000). The morphology of the catalysts was studied by a transmission electron microscope (TEM, JEOL 2010) operating at 200 kV. The WC content was determined by energy dispersive spectroscopy (Oxford, UK). The nitrogen adsorption and desorption isotherms at −196 °C were measured using a Micrometrics TriStar II 3020 system. BET surface areas were estimated over a relative pressure (P/P_0) range from 0.05 to 0.30.

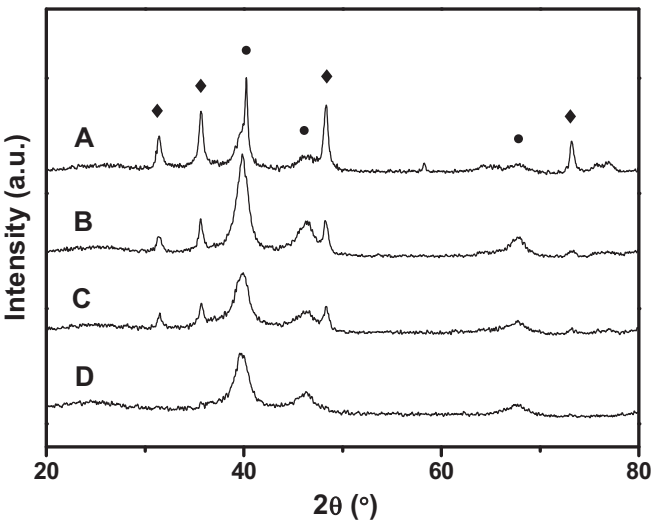

Fig. 1. XRD patterns of the as-prepared catalysts: (A) Pt/WC/C; (B) Pt/WC/C_{10}; (C) Pt/WC/C_{20}; (D) Pt/VC. Note: (♦) for WC peaks, (●) for Pt peaks.

The electrochemical measurements were carried out in a conventional three-electrode cell using a potentiostat/galvanostat (Autolab PGSTAT30) at 25 °C. A glassy carbon electrode (GCE, 5 mm in diameter) was used as the working electrode, a platinum wire as the counter electrode, and a saturated calomel electrode [SCE, 0.241 V *versus* standard hydrogen electrode (SHE)] as the reference electrode. A salt bridge with a Luggin capillary was connected to the reference electrode. To load the electrocatalyst suspension onto GCE, the electrocatalyst powder was ultrasonically mixed in ethanol to form a homogeneous ink with the catalyst concentration of 5 mg mL^{-1}, followed by dropping 10 μL of the electrocatalyst ink onto the surface of GCE. Then, 10 μL 0.5 wt.% Nafion solution was coated onto the surface to fix the electrocatalyst. All electrochemical potentials reported in the present study were given *versus* the SHE reference electrode. The electrocatalytic activity for MOR was characterized by the CV measurements at 25 °C in a nitrogen-purged 0.5 M H_2SO_4 + 0.5 M methanol solution at a scan rate of 50 mV s^{-1}. The stability was examined by a CA test at 25 °C under a constant potential of 0.6 V. For each sample, we tested for at least five times, and found that the experimental errors in the electrochemical results for catalyst performance were less than 2%. Therefore, in the present study, we report electrochemical performance directly using average values of experiment results.

3. Results and discussion

The XRD patterns are used to determine the presence of crystalline Pt on the supports and the average crystallite sizes of the WC. As shown in Fig. 1, the diffraction peaks representing a simple hexagonal phase of WC are observed at 31.4° (0 0 1), 35.6° (1 0 0) and 48.3° (1 0 1) from the different WC/C_x supports. The peaks around 40.1° (1 1 1), 46.4° (2 0 0) and 67.5° (2 2 0) indicate that Pt is loaded on to the supports. There are no impurity peaks corresponding not only to tungsten trioxide or metallic tungsten, but also to W_2C (hcp-phase) and WC_{1-x} (fcc-phase). The last two

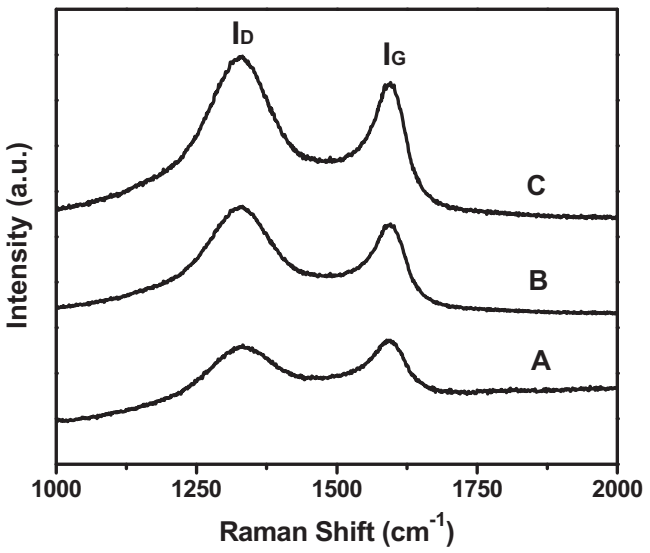

Fig. 2. Raman spectra for the catalyst supports: (A) WC/C; (B) WC/C_{10}; (C) WC/C_{20}.

peaks for tungsten carbides are common impurities observed if the preparation conditions are not carefully controlled [36,37].

The Raman spectra for the graphitic modes of carbon in the WC/C_x composites are shown in Fig. 2. It is indicated that the carbon exists in both graphitic and non-graphitic forms [16]. The spectra contain two main peaks at 1594 (G band) and 1340 cm^{-1} (D band). The G band corresponds to the E_{2g} vibration of graphitic carbon with a sp^2 electronic configuration. On the other hand, the D band is associated to the A_{1g} mode of diamond-like carbon with a sp^3 configuration. The graphitic degree of a carbon material is evaluated by using the relative intensity ratio of G band (I_G) to D band (I_D) [38]. It is worth noting that the I_G/I_D ratios of carbon in the various supports decreased with increasing the carbon content, which is consistent with the phenomenon observed by Nakamizo et al. [39]. The I_G/I_D ratio for WC/C was calculated to be 1.17 (>1), which indicates that the carbon in the WC/C composite has a well defined crystalline structure.

The nitrogen adsorption–desorption isotherms of the as-prepared catalyst supports are shown in Fig. 3. The adsorption isotherms were measured at −196 °C, by gradually increasing the

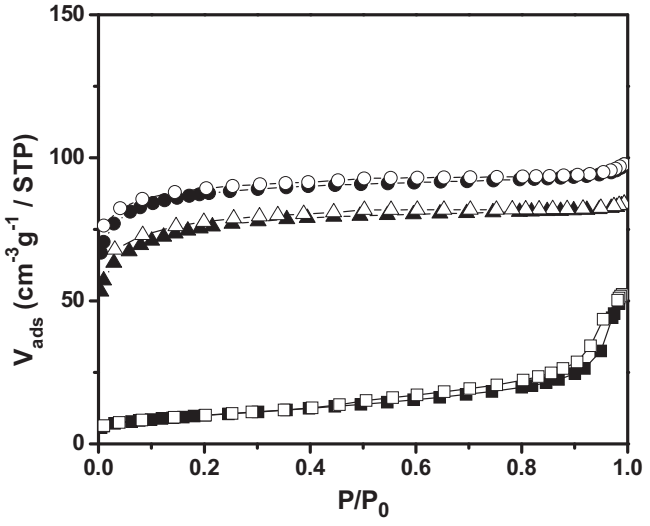

Fig. 3. Adsorption (solid symbols) and desorption (open symbols) isotherms of nitrogen for the catalyst supports: WC/C (□), WC/C_{10} (△), WC/C_{20} (○).

Table 1
The properties of the as-prepared WC/C_x composite supports.

Catalyst supports	Crystallite size[a] (nm)	I_G/I_D	BET surface area ($m^2\ g^{-1}$)	WC:C molar ratio[b]
WC/C	12.6	1.17	85.8	1:1.5
WC/C_{10}	9.2	0.85	256.8	1:11
WC/C_{20}	8.4	0.83	294.6	1:21.6

[a] Calculated by XRD.
[b] Obtained by EDS.

nitrogen pressure, P, from zero up to the saturation pressure, P_0. The initial part of the curves can be attributed to monolayer–multilayer adsorption. The capillary condensation of all the samples conformably occurs at a high pressure, around P/P_0 = 0.8–1.0, indicating a loose accumulation of nanoparticles with high surface area. It is found that the heights of the hysteresis loops are different with the variation of WC content. Evidently, the hysteresis loop increases with decreasing the WC content. The BET surface area is 85.8 $m^2\ g^{-1}$ for WC/C, and significantly increases to 294.6 $m^2\ g^{-1}$ for WC/C_{20}, which is higher than 267 $m^2\ g^{-1}$ of the commercial Vulcan XC-72 [40,41].

The properties of the different WC/C_x supports are summarized in Table 1. The WC contents in the supports are analyzed by EDS. The final molar ratios of WC:C are slightly lower than the nominal values, which could be due to the fact that the small amounts of uncarbonized metallic tungsten or tungsten oxides are removed in the alkali treatment process. As calculated by Scherrer equation choosing the WC (0 0 1) peaks [42–44], the crystallite size of WC slightly decreases with increasing the carbon content, which could be due to the relatively large carbon content that would facilitate the dispersion of W precursors and restrain the growth of WC particles. The results indicate that the nanostructured WC/C_x composites have been in situ synthesized using the microwave heating method.

The TEM images and EDS spectra of the different catalysts are shown in Fig. 4 and the size distribution of Pt is given in Fig. 5. In the case of Pt/WC/C, the average particle size is 5.4 ± 2 nm and the dispersion of Pt is characterized by a broad distribution with a large number of aggregates (Fig. 4a). The low specific surface area of supporting materials is not preferable for obtaining a fine dispersion of catalysts [45,46]. The Pt particles densely cover the WC/C surfaces but do not form bigger particles, as confirmed by the high resolution TEM images (Fig. 4b). For Pt/WC/C_{10} and Pt/WC/C_{20}, the average particle sizes of Pt are 4.0 ± 1 and 3.0 ± 1 nm, respectively. The reduction in the Pt particle size could be due to the increase in the specific surface area of the catalyst supports. The Pt particle size in the Pt/VC catalyst is around 2.8 ± 1 nm. The particle sizes of Pt on the different supports obtained by TEM agree quite well with the results calculated by XRD using the Pt (1 1 1) peaks (see Table 2).

The electrocatalytic activity of the Pt catalysts on the different supports for MOR was examined at 25 °C. The CV curves are shown in Figs. 6 and 7 for the catalysts in a nitrogen-saturated 0.5 M H_2SO_4 solution in the absence and presence of 1.0 M CH_3OH, respectively. We tested each sample for at least five times and took the average value. In the CV curves measured in the 0.5 M H_2SO_4 solution (Fig. 6), the hydrogen adsorption/desorption area is used to evaluate the electrochemical surface area (ECSA). A higher ECSA normally represents more activation sites for hydrogen adsorption/desorption, which is preferred not only for hydrogen oxidation but also for methanol oxidation, because the MOR also involves hydrogen adsorption/desorption step. The obtained ECSA values are summarized in Table 2. The Pt on the WC/C_x composite supports shows much higher ECSA values than that (297.4 $cm^2\ mg^{-1}$) of the Pt/VC. In terms of the TEM and XRD measurements, the particle sizes of Pt supported on carbon black XC-72 are smaller than those

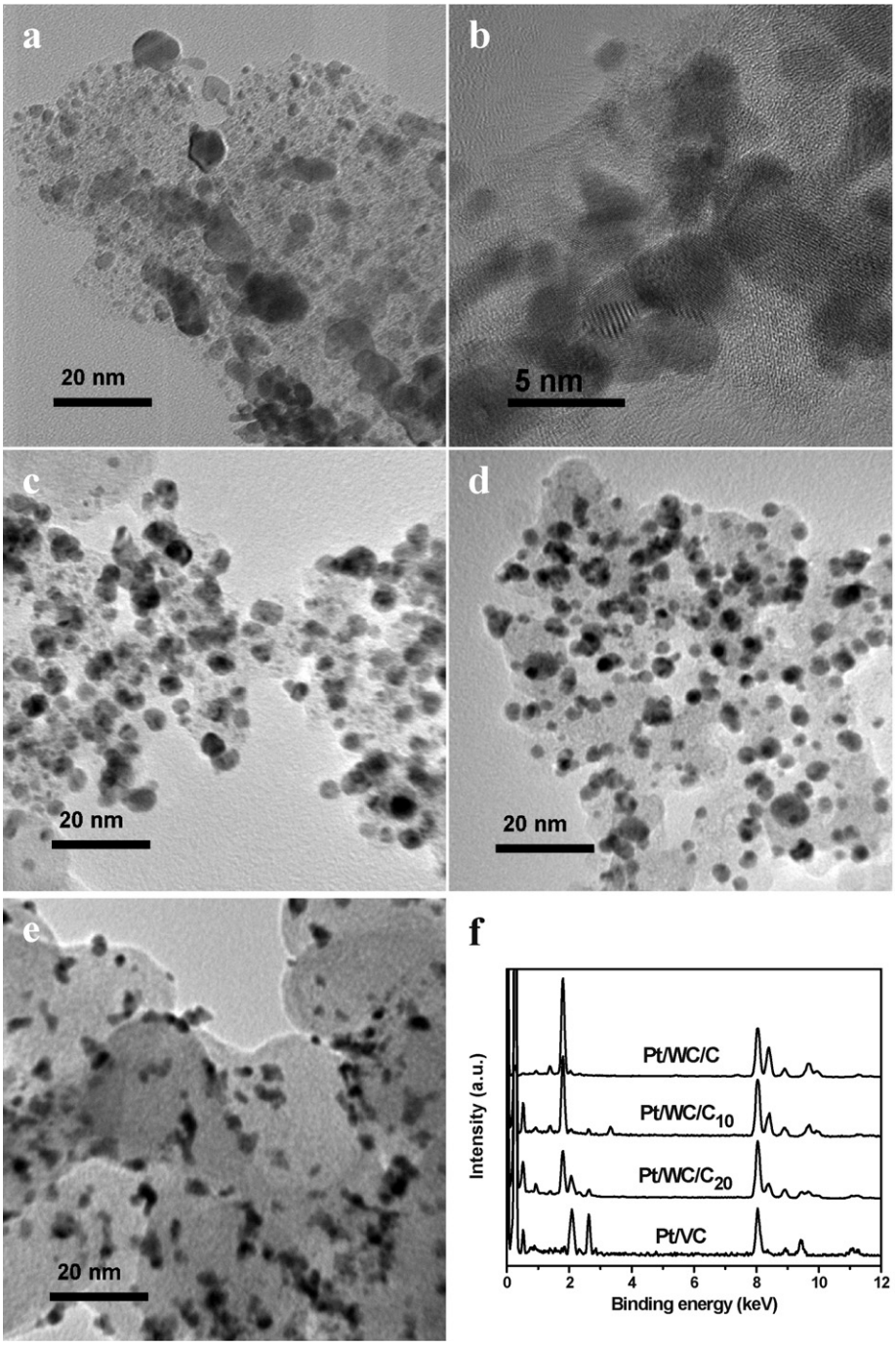

Fig. 4. TEM images of (at (a) low and (b) high magnifications) Pt/WC/C; (c) Pt/WC/C_{10}; (d) Pt/WC/C_{20}; (e) Pt/VC; (f) EDS spectra of the different catalysts.

of Pt supported on the WC/C_x materials. Generally, the smaller the particle sizes of Pt catalysts, does the higher ECSA. However, the Pt/WC/C_x catalysts show higher ECSA values than that of Pt/VC. The reason is due to the fact that the WC is able to participate in the hydrogen adsorption/desorption step so that the ECSA values of the Pt/WC/C_x catalysts are enhanced. The similar interplay between Pt and WC is also observed for electrooxidation of methanol on Pt/WC [47–49]. Tungsten carbide alone without Pt shows a low activity

Table 2
The properties and electrochemical parameters of the different catalysts.

Catalyst	Pt particle size (nm)	ECSA ($cm^2\ mg^{-1}$)	Onset potential (V)	Peak current ($mA\ mg^{-1}$)	Peak potential (V)	Ratio (I_f/I_b)
Pt/WC/C	4.8	368.2	0.58	260	0.84	1.13
Pt/WC/C_{10}	4.0	423.6	0.58	313	0.84	1.08
Pt/WC/C_{20}	3.2	405.8	0.62	275	0.86	1.02
Pt/VC	3.3	297.4	0.62	198	0.86	0.68

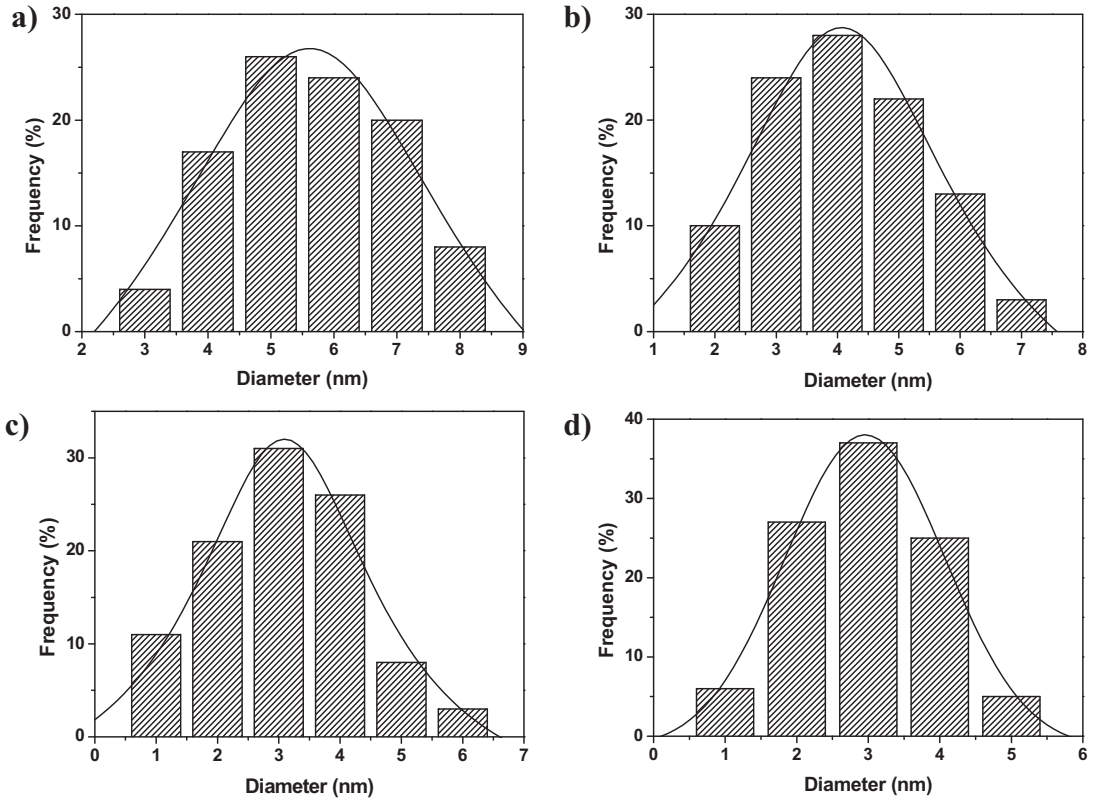

Fig. 5. Histograms of size distribution of Pt particles in (a) Pt/WC/C, (b) Pt/WC/C_{10}, (c) P/WC/C_{20}, and (d) Pt/VC.

under the same reaction conditions. Thus hydrogen may adsorb first on Pt and then migrate to the WC surface probably by a hydrogen spillover mechanism [50,51]. The electrooxidation of hydrogen then takes place on both Pt and WC, giving a higher activity than that obtained from Pt alone. The ECSA of the Pt/WC/C_{10} is higher than Pt/WC/C, most likely due to the smaller size and much better dispersion of Pt nanoparticles on WC/C_{10}. On the other hand, the ECSA of the Pt/WC/C_{20} is smaller than Pt/WC/C_{10}. This is because the WC particles in the WC/C_{20} support may be partially capped or surrounded by the excessive carbon so that some of them become electrochemically unaccessible.

The methanol oxidation activity is reflected by the magnitude of the anodic peak current in the forward scan while the peak in the reverse scan is due to the reactivation of Pt associated with the removal of residual carbon species [52]. As shown in Fig. 7, in the forward scan, the onset potential on Pt/WC/C and Pt/WC/C_{10} is 0.58 V, showing a negative shift as compared to 0.62 V of Pt/WC/C_{20} and Pt/VC. Their peak potentials for MOR are located at 0.84 V for Pt/WC/C and Pt/WC/C_{10}, and 0.86 V for Pt/WC/C_{20} and Pt/VC catalysts. The mass catalytic activities (reflected by peak current density, which have been normalized to the Pt loading) are 198, 260, 313 and 275 mA mg^{-1} for Pt/VC, Pt/WC/C, Pt/WC/C_{10} and

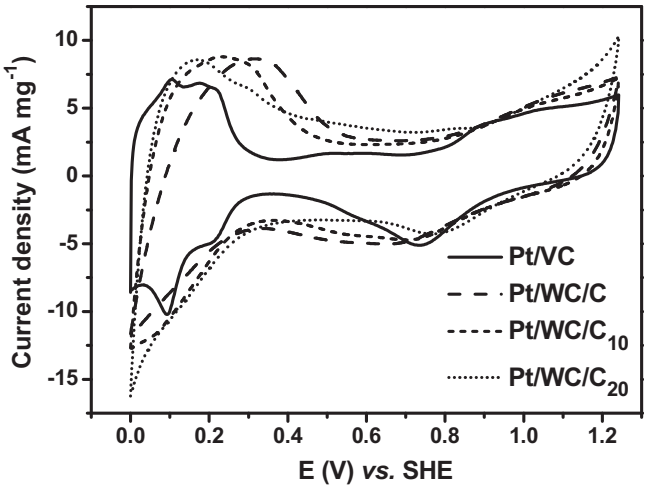

Fig. 6. Mass-normalized CV curves of the different catalysts in a N_2-saturated 0.5 M H_2SO_4 solution at a scan rate of 20 mV s^{-1}.

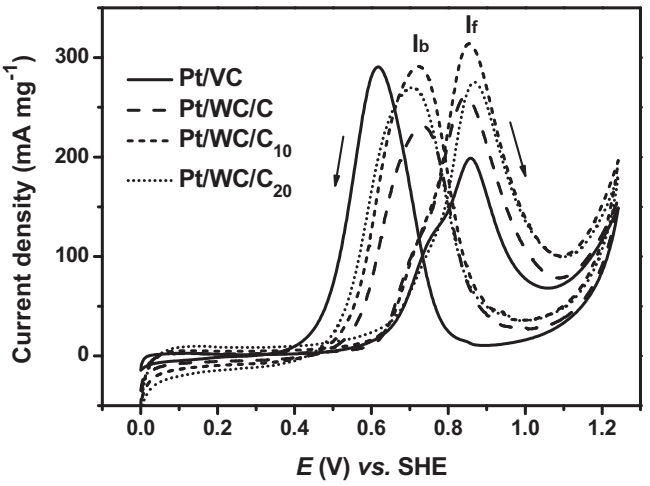

Fig. 7. Mass-normalized CV curves of the different Pt catalysts in a N_2-saturated 0.5 M H_2SO_4 + 1 M CH_3OH solution at a scan rate of 50 mV s^{-1}.

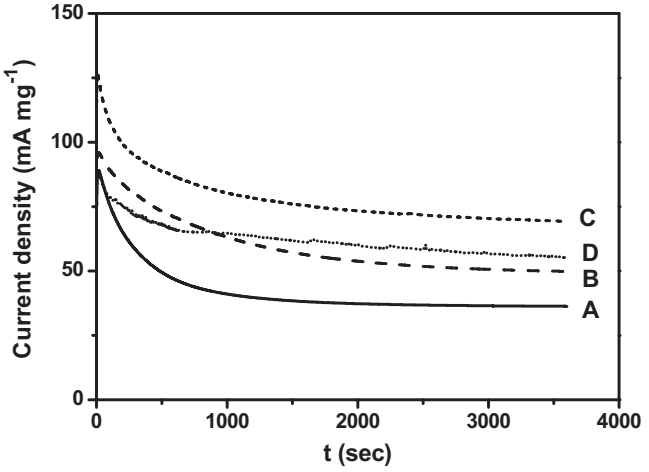

Fig. 8. CA curves for (A) Pt/VC, (B) Pt/WC/C, (C) Pt/WC/C_{10} and (D) Pt/WC/C_{20} catalysts in a N_2-saturated 0.5 M H_2SO_4 + 1 M CH_3OH solution at a constant potential of 0.6 V.

Pt/WC/C_{20}, respectively. The Pt/WC/C, Pt/WC/C_{10} and Pt/WC/C_{20}, respectively, exhibit 31.3%, 58.1% and 38.9% improvements in catalytic activity as compared to the Pt/VC. The best catalytic activity is obtained on Pt/WC/C_{10}. The results show that the content of WC has a great impact on the performance of the electrocatalysts. The lower specific surface area of the WC/C supporting materials results in the relatively poor dispersion of Pt nanoparticles, decreasing the utilization efficiency of Pt catalysts. On the other hand, because Pt particles are selectively deposited on the WC surfaces as investigated by Jeon et al. [23], some WC particles in the WC/C_{20} composite have been shielded by a passive carbon film, resulting in a lower contribution of WC to the MOR. The Pt/WC/C_{10} catalyst shows the highest mass activity and relatively low onset potential, which are desirable for MOR [25]. Further reducing the Pt particle size would enhance the catalytic activity. The current peak ratio of I_f (the forward peak current density)/I_b (the backward peak current density) could be used to express the CO tolerance on Pt surface. A higher I_f/I_b ratio means a better CO tolerance. The I_f/I_b ratios are 0.68, 1.13, 1.08 and 1.02 for Pt/VC, Pt/WC/C, Pt/WC/C_{10} and Pt/WC/C_{20}, respectively. The Pt/WC/C, Pt/WC/C_{10} and Pt/WC/C_{20} catalysts, respectively, show 66.2%, 58.8% and 50.0% improvements in the I_f/I_b ratio over the Pt/VC. This result further demonstrates the enhanced CO tolerance on Pt/WC/C_x catalysts. The positive effect of WC is obvious and the performance improvement can be explained by a synergistic effect between Pt and WC nanoparticles [27]. The electrooxidation of methanol is a very complex reaction involving many intermediate species that may poison the Pt by blocking active sites for the further reactions. In the presence of Pt, WC is active in electrochemical methanol oxidation and water decomposition [47,48]. The formation of hydroxyl groups from water activation is essential for removing the metal-poisoning CO molecules from the surfaces of catalysts.

The stability of the catalysts is evaluated by a CA method at a constant potential 0.6 V and the results are shown in Fig. 8. As can be seen, there is a continuous current drop with testing time, which is very rapid at the initial stage, followed by a much slower decay. The rapid current decay represents the poisoning effect on the catalyst surface. The Pt/VC catalyst shows the fastest decrease among these catalysts, indicating the lowest tolerance to CO or carbonaceous intermediates formed during the MOR. The Pt/$WC/_{10}$ catalyst exhibits the highest stability due to the synergy between Pt and WC, as discussed above.

4. Conclusions

In summary, nanostructured WC/C_x composites that can act as efficient catalyst supports for the MOR are synthesized in situ using water soluble carbon and tungsten precursors by a microwave heating method. It is found that the WC crystallite size decreases with increasing the carbon content. The performances of the Pt/WC/C_x catalysts for MOR are studied and evaluated in acid media. The Pt/WC/C_x catalysts exhibit higher activity and stability than does the Pt/VC catalyst. This result is considered to be due to a synergy between Pt and the WC/C_x support in promoting the MOR. Further, the activity of the Pt/WC/C_x catalysts is affected by the WC content and structure of the WC/C_x supports, with Pt/WC/C_{10} showing a higher performance than Pt/WC/C or Pt/WC/C_{20}. The superiority of Pt/WC/C_{10} is thought to be due to the Pt/WC synergy and the better utilization of Pt surface in the composite.

References

[1] H. Liu, C. Song, L. Zhang, J. Zhang, H. Wang, D.P. Wilkinson, Journal of Power Sources 155 (2006) 95–110.
[2] S. Wang, X. Wang, S.P. Jiang, Langmuir 24 (2008) 10505–10512.
[3] S. Wasmus, A. Kuver, Journal of Electroanalytical Chemistry 461 (1999) 14–31.
[4] C. Bianchini, P.K. Shen, Chemical Reviews 109 (2009) 4183–4206.
[5] J. Lu, S. Lu, S.P. Jiang, Chemical Communications 47 (2011) 3216–3218.
[6] J. Lu, H. Tang, S. Lu, H. Wu, S.P. Jiang, Journal of Materials Chemistry 21 (2011) 6668–6676.
[7] M.B. Zellner, J.G. Chen, Journal of the Electrochemical Society 152 (2005).
[8] C. Bianchini, V. Bambagioni, J. Filippi, A. Marchionni, F. Vizza, P. Bert, A. Tampucci, Electrochemistry Communications 11 (2009) 1077–1080.
[9] J. Lu, S. Lu, D. Wang, M. Yang, Z. Liu, C. Xu, S.P. Jiang, Electrochimica Acta 54 (2009) 5486–5491.
[10] J.L. Lu, C. Xu, S.P. Jiang, International Journal of Nanoscience 8 (2009) 203–207.
[11] Y. Shao, J. Liu, Y. Wang, Y. Lin, Journal of Materials Chemistry 19 (2009) 46–59.
[12] C. Wang, M. Waje, X. Wang, J.M. Tang, R.C. Haddon, Y. Yan, Nano Letters 4 (2004) 345–348.
[13] C.A. Bessel, K. Laubernds, N.M. Rodriguez, R.T.K. Baker, Journal of Physical Chemistry B 105 (2001) 1115–1118.
[14] W.C. Choi, S.I. Woo, M.K. Jeon, J.M. Sohn, M.R. Kim, H.J. Jeon, Advanced Materials 17 (2005) 446–451.
[15] B.E. Roustom, G. Foti, C. Comninellis, Electrochemistry Communications 7 (2005) 398–405.
[16] S. Shanmugam, A. Gedanken, Small 3 (2007) 1189–1193.
[17] H. Chhina, S. Campbell, O. Kesler, Journal of Power Sources 161 (2006) 893–900.
[18] H. Chhina, S. Campbell, O. Kesler, Journal of Power Sources 164 (2007) 431–440.
[19] H. Chhina, S. Campbell, O. Kesler, Journal of the Electrochemical Society 154 (2007).
[20] H. Chhina, S. Campbell, O. Kesler, Journal of Power Sources 179 (2008) 50–59.
[21] L. Hu, S. Ji, Z. Jiang, H. Song, P. Wu, Q. Liu, Journal of Physical Chemistry C 111 (2007) 15173–15184.
[22] S. Cahen, G. Furdin, J.F. Marêche, A. Albiniak, Carbon 46 (2008) 511–517.
[23] M.K. Jeon, K.R. Lee, W.S. Lee, H. Daimon, A. Nakahara, S.I. Woo, Journal of Power Sources 185 (2008) 927–931.
[24] R. Wang, C. Tian, L. Wang, B. Wang, H. Zhang, H. Fu, Chemical Communications (2009) 3104–3106.
[25] R. Ganesan, D.J. Ham, J.S. Lee, Electrochemistry Communications 9 (2007) 2576–2579.
[26] Z. Zhao, X. Fang, Y. Li, Y. Wang, P.K. Shen, F. Xie, X. Zhang, Electrochemistry Communications 11 (2009) 290–293.
[27] Y. Hara, N. Minami, H. Matsumoto, H. Itagaki, Applied Catalysis A: General 332 (2007) 289–296.
[28] F. Hu, G. Cui, Z. Wei, P.K. Shen, Electrochemistry Communications 10 (2008) 1303–1306.
[29] F.P. Hu, P.K. Shen, Journal of Power Sources 173 (2007) 877–881.
[30] M. Nie, P.K. Shen, Z. Wei, Journal of Power Sources 167 (2007) 69–73.
[31] M. Nie, P.K. Shen, M. Wu, Z. Wei, H. Meng, Journal of Power Sources 162 (2006) 173–176.
[32] M. Nie, H. Tang, Z. Wei, S.P. Jiang, P.K. Shen, Electrochemistry Communications 9 (2007) 2375–2379.
[33] E.J. Rees, K. Essaki, C.D.A. Brady, G.T. Burstein, Journal of Power Sources 188 (2009) 75–81.
[34] D. Wang, S. Lu, S.P. Jiang, Chemical Communications 46 (2010) 2058–2060.
[35] D. Wang, L. Zhuang, J. Lu, Journal of Physical Chemistry C 111 (2007) 16416–16422.
[36] D.J. Ham, Y.K. Kim, S.H. Han, J.S. Lee, Catalysis Today 132 (2008) 117–122.
[37] Q. Zhu, S. Zhou, X. Wang, S. Dai, Journal of Power Sources 193 (2009) 495–500.
[38] F. Tuinstra, J.L. Koenig, Journal of Chemical Physics 53 (1970) 1126–1130.
[39] M. Nakamizo, R. Kammereck, P.L. Walker Jr., Carbon 12 (1974) 259–267.
[40] C. Lamy, A. Lima, V. LeRhun, F. Delime, C. Coutanceau, J.M. Léger, Journal of Power Sources 105 (2002) 283–296.

[41] W. Li, C. Liang, W. Zhou, J. Qiu, Z. Zhou, G. Sun, Q. Xin, Journal of Physical Chemistry B 107 (2003) 6292–6299.
[42] T. Hyde, Platinum Metals Review 52 (2008) 129–130.
[43] J.D. Kamminga, L.J. Seijbel, Journal of Research of the National Institute of Standards and Technology 109 (2004) 65–74.
[44] T. Ungár, J. Gubicza, G. Ribárik, A. Borbély, Journal of Applied Crystallography 34 (2001) 298–310.
[45] L. Yang, Y. Qi, X. Yuan, J. Shen, J. Kim, Journal of Molecular Catalysis A: Chemical 229 (2005) 199–205.
[46] D. Zhao, Q. Huo, J. Feng, B.F. Chmelka, G.D. Stucky, Journal of the American Chemical Society 120 (1998) 6024–6036.
[47] R. Ganesan, J.S. Lee, Angewandte Chemie-International Edition 44 (2005) 6557–6560.
[48] R. Ganesan, J.S. Lee, Journal of Power Sources 157 (2006) 217–221.
[49] M.K. Jeon, H. Daimon, K.R. Lee, A. Nakahara, S.I. Woo, Electrochemistry Communications 9 (2007) 2692–2695.
[50] L. Chen, A.C. Cooper, G.P. Pez, H. Cheng, Journal of Physical Chemistry C 111 (2007) 18995–19000.
[51] L. Chen, A.C. Cooper, G.P. Pez, H. Cheng, Journal of Physical Chemistry C 112 (2008) 1755–1758.
[52] F. Su, Z. Tian, C.K. Poh, Z. Wang, S.H. Lim, Z. Liu, J. Lin, Chemistry of Materials 22 (2010) 832–839.